# Flight Simulator Evaluation of Fuel-Efficient Arrival Profiles

Ramon Andreu Altava, Jean Claude Mere, Pierre Neri, Daniel Delahaye, Thierry Miquel

# Flight Simulator Evaluation of Fuel-Efficient Arrival Profiles

Ramon Andreu Altava *, Jean Claude Mere† and Pierre Neri‡
*Airbus Operations SAS, Toulouse, 31300, France*

Daniel Delahaye§ and Thierry Miquel¶
*ENAC, University of Toulouse, 31400, France*

## Nomenclature

| | | |
|---|---|---|
| $CI$ | = | Cost Index [lb/s] |
| Conf | = | Flap setting [−] |
| $D$ | = | Aerodynamic drag force [lbf] |
| $ds$ | = | Distance span [ft] |
| $ESF$ | = | Energy Share Factor [−] |
| $E_{T_s}$ | = | Specific total energy [ft] |
| $E_{k_s}$ | = | Specific potential energy [ft] |
| $E_{p_s}$ | = | Specific kinetic energy [ft] |
| $\dot{m}$ | = | Fuel flow rate [lb/s] |
| $g_0$ | = | Gravitational constant, 32.174 [ft/s$^2$] |
| $h$ | = | Geometric altitude [ft] |
| $m$ | = | Aircraft mass [lb] |
| $s$ | = | Aircraft distance [ft] |
| $t$ | = | Flight time [s] |
| $Thr$ | = | Thrust force [lbf] |
| $TSP$ | = | Thrust Setting Parameter [−] |
| $V$ | = | True airspeed [ft/s] |
| $V_w$ | = | Wind airspeed [ft/s] |
| $\Delta$ISA | = | Temperature deviation [°K] |
| $\delta_{ab}$ | = | Airbrakes position [−] |
| $\gamma$ | = | Aerodynamic flight-path angle [rad] |
| $\gamma_T$ | = | Total flight-path angle [rad] |

*PhD candidate, Navigation Systems, Airbus.
†Flight Management System engineer, Navigation Systems, Airbus.
‡Flight Management System engineer, Navigation Systems, Airbus.
§Head of Optim group, ENAC.
¶PhD, Optim group, ENAC.

# I. Introduction

Air traffic continued growth in the last decades and predictions for the coming years [1] require a modernization of current air transportation system. The increased number of operations results in the congestion of airspaces with the consequent propagation of delays [2]. The environmental footprint of aviation industry already constitutes 3.6 % of the total European greenhouse emissions [3]. Noise levels in the vicinity of airports have decreased by 14% per flight due to technological improvements on aircraft, nevertheless the average noise exposure grows [3] because of air traffic increase. Moreover, other factors such as jet fuel prices volatility and airlines strong market competition promote flight efficiency as a central topic for research.

In recent years, flight efficiency has been largely improved through initiatives such as Free Route Airspace [4] or the introduction of Continuous Descent Operations (CDO) [5], which have demonstrated to be generally more efficient than conventional step-down operations in terms of noise and gas emissions [6]. In major airports surrounded by large residential areas, airspace designers have introduced noise abatement procedures based on CDO that are operated during certain periods of time, usually in nighttime. Similarly, novel Area Navigation (RNAV) design procedures in the United States contain a set of window altitude constraints located higher than usual, which define a descent corridor enabling CDO. Furthermore, the complex environment in descent and approach phases represents a high level of workload for pilots, and complicates the optimal management of aircraft trajectory with a consequent impact on flight efficiency. This Note proposes an onboarded function that generates permanent optimal trajectories based on enhanced energy management. The term permanent refers to the continuous availability of a trajectory linking the destination airport to the current aircraft position regardless of the current guidance mode and energy condition. Hence, the provision of the optimal trajectory accounting for the aircraft energy condition supports flight crews decision-making processes and pave the route for advanced automation capabilities in the future.

The Flight Management System (FMS) entered into service in the early 1980s [7] and decreased navigation workload in a manner that reduced flight crews from three members to two. The system performs relevant functions [8] such as navigation, flight planning (both lateral and vertical), performance computations and provision of guidance and display commands. This Note focuses on descent and approach operations where state-of-the-art FMS compute a vertical profile based on the lateral path defined by an entered arrival procedure and other parameters such as Cost Index (CI), cruise flight level and an estimation of the mass at the destination. The profile is constructed upstream from the runway threshold until the cruise altitude, and consist of a concatenation of idle and geometric segments, the latter being constructed as soon as an altitude constraint restricts the construction of the idle path. Depending on the nature of the altitude constraints, geometric segments require either auto-thrust adjustments to maintain a speed target in shallow paths or airbrakes extension in steep segments, while the elevator guides the aircraft through the vertical path.

In contrast, idle segments set auto-thrust to idle whilst the elevator maintains the target speed. Based on the CI selected by the pilot, the FMS computes the optimal Mach and CAS descent speeds, used as target speeds by the guidance law, except otherwise prescribed by the airline. The transition from Mach to CAS occurs at the crossover altitude, defined as the altitude at which the Mach/CAS coupling has the same value of true airspeed (TAS). Below the tropopause and above the crossover altitude, the aircraft descends at constant Mach while CAS increases. Below the crossover altitude, optimal CAS speed is maintained constant until any other speed restriction applies whereas Mach decreases gradually. The path is constructed through the integration of the equations of motion and decelerations are computed by a fixed Energy Share Factor (ESF), which distributes the available energy between altitude and speed, permitting the aircraft to descend and decelerate at the same time. In traditional step-down approaches, aircraft deceleration to approach speed is performed in a level-flight located at the glide-slope capture altitude whereas, in the frame of CDO, aircraft decelerate and change flap configurations as they descend. The main limitation of this approach is that depending on the aircraft performance and the arrival procedure, deceleration to approach speed might be initiated too soon, in certain cases well above 7000 feet. This situation leads to long approach procedures in which flaps are extended quite far away from the destination runway, which in some cases require more fuel than conventional step-down profiles. Therefore, current FMS hypotheses are valid for the construction of any arrival procedure but the resulting trajectory is not necessarily optimal. The first enhancement to the current FMS design proposed in this Note is to consider other types of segments for the profile construction, whose choice depends on the selected arrival procedure. These segments may require to fly at economic speeds other than those used by the traditional Mach/CAS descent law. This suggests that fuel consumption can be reduced by following variable CAS profiles instead of constant CAS profiles as prescribed by airlines standard operating procedures.

The provision of radar vectors from ATC, unexpected wind errors or biased mass estimations are the most probably causes for profile deviations from the intended routes [9]. In these situations, the FMS profile is not recomputed to take into consideration the current aircraft energy condition, but flight crews adapt the flight strategy according to their own criterion. The aircraft energy condition is defined as the sum of potential and kinetic energy so that high-energy occurs when the aircraft is too fast, too high or both, while low-energy situations imply that the aircraft is low or below its target speed [10]. In flight operations, the term energy management refers to the continuous transformation of energy that occurs due to the use of flight controls as the aircraft descends to the destination. In the absence of a valid reference trajectory, pilots are responsible for managing aircraft energy state through power and control devices such as thrust levers, airbrakes, landing gear and flap settings that modify the aircraft energy rate. The second enhancement to the FMS design proposed in this Note is the continuous recomputation of the optimal trajectory on the basis of current aircraft position. This is the concept of the permanent trajectory, where the calculation always reaches the aircraft position independently of the current energy state or flight mode, and applies the necessary energy management strategy to dissipate any excess of energy during the approach. The permanent trajectory is a relevant concept as it not only helps

pilots in energy management decision-making processes but also would permit to completely automate the approach phase and therefore constitute a significant improvement to flight efficiency.

Trajectory optimization is usually formulated as an optimal control problem [11] solved through direct, indirect or dynamic programming methods [12]. Past works have solved the problem through pseudo-spectral methods, as it is the case for the Time and Energy Management Operations [13] function that minimizes the number of energy corrections to compensate wind errors and satisfy a time constraint. Indirect methods are implemented in the real-time algorithm proposed in [14], whose results are compared with a FMS under different wind conditions [15]. While most works optimize fuel consumption, others focus on the minimization of noise and pollutant emissions [16]. Low noise augmentation system presented in [17] computes dynamically airbrakes, landing gear and flap settings extension in order to stabilize the aircraft whilst minimizing noise impact. The function has been embarked on an electronic flight bag and has been successfully tested in flight. A* algorithm [18] has been successfully implemented in [19], [20] and [21] to compute optimal trajectories, although these works rely on simple heuristic functions that represent no advantage with regard to classic Dijkstra's algorithm [20]. Other methods like energy-optimal path-tracking algorithm introduced in [22] and [23] optimize the descent and approach due to the minimization of the energy path and proposes a relation between flight time and fuel consumption [24]. Energy-state approximations have also been applied to aircraft trajectory optimization in works such as [25] and [26]. A benchmark of optimality between fuel and time is proposed in [27] and [28], the trajectories being constructed by comparing different energy sharing ratios. Energy-state approximations based on an aircraft total energy formulation [29] often consider energy as the independent or the control variable. Even if works such as [11][26],[27] and [28] provide fair approximations to trajectory optimization problems, bounds on states and controls are seldom included in the solution. Instead, constraints such as idle thrust are often imposed. As a result, these algorithms are not representative of real operations. In today's operations, aircraft follow published procedures dictated by airspace designers, which consists in a concatenation of altitude and speed constraints. On top of that, airlines prescribe their own procedure constraints for reasons of safety, passenger comfort and efficiency. The whole set of constraints restrict the optimization process, requiring high computational capacity to solve these problems. Those works in the literature integrating constraints usually solve typical descent profiles, based on a series of consecutive segments, instead of particular arrival procedures. This converts the initial two-point boundary value problem into a multi-phase optimal control problem, most of the time yielding to local optimal solutions. The lack of generality of those algorithms implies that they may not applicable to other operational procedures. This Note extends previous works as it proposes a generic algorithm that solves any combination of state, control and path constraints, so it is applicable to any existing arrival procedure. It is is based on A* [18] algorithm, which is a deterministic and efficient numerical technique that computes iteratively the global optimum solution. Moreover, it is relatively simple to implement, which makes it desirable for being integrated in the next generation of FMS. The algorithm yields the

global optimum solution as long as it exists, the computed trajectory accounting for the current aircraft position. This Note extends the previous work presented in [30] by comparing the obtained results with a real certified FMS. Then, the obtained optimal trajectory is operationally assessed in the flight simulator, with the aim of validating the feasability of the computed profile and fuel savings.

The outline of this Note is the following: the mathematical formulation of the problem is presented in section II whereas the main functioning principles of the algorithm are described in section III. Then, section IV discusses the results obtained for the presented case study. Then, the trajectory computed by the algorithm is compared with the one produced by a certified FMS and tested in a flight simulator. Finally, section V concludes the study and establishes directions for future research.

## II. Mathematical Formulation

### A. Optimization Problem

The aircraft motion in the vertical plane is represented by a point-mass model that provides a sufficient level of representativeness [31] from a performance perspective. The generation of the trajectory focuses on slow dynamics variables and disregards fast dynamics such as flight-path angle rate ($\dot{\gamma}$). The objective function is the minimization of fuel consumption along the trajectory, which is given by the following expression:

$$J = \min \int_{s_0}^{s_f} \left(\dot{m} + \mathrm{CI}\right) \frac{1}{V\cos\gamma + V_w}\, ds \tag{1}$$

Where $\dot{m}$ is fuel flow rate, CI the Cost Index, $V$ the aircraft true airspeed, $V_w$ the wind speed, $\gamma$ the aerodynamic flight-path angle, $s_0$ the initial distance at the stabilization gate and $s_f$ is the target distance. The CI is defined as the ratio between the unit cost of time (\$/s) and the unit cost of fuel (\$/kg). Hence, a CI equal to zero leads to the fuel minimization problem. The algorithm computes optimal trajectories by means of an Airbus genuine Performance database (PDB) containing engine, aerodynamic and other performance data. The engine model contains thrust maximum and minimum (idle) settings whose use depends on the flight phase. The thrust setting parameter (TSP) gives the percentage of the maximum thrust used by the engine, which is computed as follows:

$$TSP = f_1(h, M) \tag{2}$$

Where $h$ is the aircraft altitude and $M$ the Mach number. Thrust ratings are computed through the TSP from Eq.(2).

$$Thr = f_2(TSP, M) \tag{3}$$

The previous process is only applicable to idle segments. In other segments where thrust is different from idle, the equations of motion give the thrust value, which replaces $Thr$ in Eq.(3) and it is then used for iterating TSP. Eventually, the fuel flow rate ($\dot{m}$) is calculated through the TSP computed by either Eq.(2) or Eq.(3):

$$\dot{m} = f_3(TSP, h, M) \tag{4}$$

**B. Aircraft Model**

This Note presents a mathematical formulation based on the total energy of the aircraft, which relates directly the altitude and the speed with the control variables. Aircraft specific energy is defined as the sum of kinetic and potential energy independent of aircraft weight. The derivative of the term with respect to time gives the energy rate or energy height:

$$\dot{E}_{T_s} = \dot{E}_{p_s} + \dot{E}_{k_s} = V \sin\gamma + \frac{V\dot{V}}{g_0} \tag{5}$$

Where $\dot{E}_{T_s}$ is the specific total energy rate, also called energy height, $\dot{E}_{k_s}$ is the specific kinetic energy rate and $\dot{E}_{p_s}$ the specific potential energy rate. The $ESF$ is defined as the percentage of the specific total energy rate attributed to deceleration in contrast to descent:

$$ESF = \frac{\dot{E}_{k_s}}{\dot{E}_{k_s} + \dot{E}_{p_s}} \tag{6}$$

The combination of Eqs.(5) and (6) leads to the following expression:

$$\sin\gamma = \frac{(1 - ESF)}{ESF} \frac{\dot{V}}{g_0} \tag{7}$$

The summation of forces acting on the aircraft in the vertical plane are given in equation (8).

$$m\dot{V} = Thr - D - mg_0 \sin\gamma \tag{8}$$

Where $Thr$ is thrust and $D$ is aerodynamic drag. The total flight-path angle or total energy angle ($\gamma_T$) is defined as the available energy rate budget to be distributed between potential and kinetic energy, thus is represented as the sum of the aerodynamic flight-path angle ($\gamma$) and the resulting acceleration:

$$\sin\gamma_T = \sin\gamma + \frac{\dot{V}}{g_0} = \frac{\sin\gamma}{1 - ESF} = \frac{Thr - D(h, V, \delta_{ab}, \text{Conf})}{mg_0} \tag{9}$$

Where $\delta_{ab}$ represents the deflection of airbrakes and Conf the aircraft flap setting. In this Note, the classic time-dependent equations of motion are converted into distance-dependent equations, since it simplifies the constraint management and both initial and final distances are known, contrary to the final time. The introduction of Eqs.(7) and

(9) combined with the small angle approximation, $\sin\gamma_T \approx \gamma_T$, result in the following formulation:

$$\begin{cases} h' = \dfrac{V\,(1-ESF)\,\gamma_T}{V\cos\gamma + V_w} \\ V' = \dfrac{g_0\;ESF\;\gamma_T}{V\cos\gamma + V_w} \\ m' = \dfrac{dm}{ds} = \dfrac{-\dot{m}}{V\cos\gamma + V_w} \\ t' = \dfrac{dt}{ds} = \dfrac{1}{V\cos\gamma + V_w} \end{cases} \tag{10}$$

In the previous formulation of equations of motion, wind gradients have been neglected. The mass of the aircraft $m$ changes as a function of the Eq.(4) whereas the flight time $t$ depends on the inverse of the ground distance. The value of $\gamma$ is assumed constant for the segment, except for long distances where a correction is made. A segment is the portion of the trajectory that links two states. The state vector of the problem can be deducted from Eq.(10).

$$x(s) = [h, V, m, t] \tag{11}$$

Then, the control variables that generate the states of Eq.(11) are defined by:

$$u(s) = [\gamma_T, ESF, \delta_{ab}, \text{Conf}] \tag{12}$$

These two control variables are independent as they are used for computing the value of $\gamma_T$, which depends on the previous two and the TSP value. Then, $ESF$ is also an independent variable that distributes the available energy given by $\gamma_T$ between the altitude and the speed. The values of $\gamma_T$ and $ESF$ compute $\gamma$ by means of Eq.(9), which is used as auxiliary variable in the equations of motion described by Eq.(10).

### C. Problem Constraints

Constraints on state variables are given by the arrival procedure design and the published altitude and speed constraints contained in the Navigation Database (NDB) [32]:

$$\begin{cases} \text{AT OR ABOVE} \rightarrow \quad h \geq h_{CSTR} \\ \text{AT OR BELOW} \rightarrow \quad h \leq h_{CSTR} \\ \text{WINDOW} \rightarrow \quad h_{CSTR_a} \geq h \leq h_{CSTR_b} \\ \text{AT} \rightarrow \quad h = h_{CSTR} \end{cases} \tag{13}$$

Where $h_{CSTR}$ is the value of the altitude constraint expressed in feet or flight level (FL), the latter represents the altitude of the aircraft at standard air pressure in hundreds of feet. For window constraints, the altitude is bounded between a lower ($h_{CSTR_a}$) and an upper ($h_{CSTR_b}$) value. Similarly, a speed constraint limits aircraft speed below a certain value:

$$V_{CAS} \leq V_{CAS_{CSTR}} \tag{14}$$

Furthermore, ATC regulation generally imposes a maximum speed of 250 kt Calibrated Airspeed (CAS) for all aircraft below FL100:

$$V_{CAS} \leq 250 \quad \forall h \leq \text{FL100} \tag{15}$$

In addition to the previous boundaries, aircraft speed shall remain within the flight envelope defined by the lowest selectable speed, which is defined as 1.23 times the stall speed at 1g load factor or $V_{LS} = 1.23V_{1g}$, and the maximum operating speed ($V_{MO}$):

$$V_{LS} \leq V_{CAS} \leq V_{MO} \tag{16}$$

During the approach phase, flap changes decrease the stall speed and the next flap Conf is limited to the maximum flap extended speed ($V_{FE}$) in order to avoid structural damage:

$$V_{LS} \leq V_{CAS} \leq V_{FE} \quad \text{if Conf} \neq clean \tag{17}$$

Longitudinal accelerations are limited to take into account passengers comfort [33] as follows:

$$\left|\frac{dV}{dt}\right| \leq 0.07 \cdot g_0 \tag{18}$$

The control variables $\gamma_T$, $ESF$ and $\delta_{ab}$ are bounded between a maximum and minimum value. The thrust required to perform a level-off at constant speed, defines the upper limit of $\gamma_T$, whilst idle thrust combined with full airbrakes extension set the lower bound:

$$\gamma_{T_{min}}\Big|_{\substack{Thr=Thr_{idle} \\ D=\delta_{ab_{\text{Full}}}}} \leq \gamma_T \leq \gamma_{T_{max}}\Big|_{Thr=D} \tag{19}$$

Climb segments ($\gamma > 0$) are forbidden per design so that $\gamma_{T_{max}}$ is always less than or equal to zero to minimize fuel consumption. The $ESF$ is then limited operationally as follows:

$$ESF \in \{-0.5, ..., 1\} \tag{20}$$

It can be observed from Eq.(6) that $ESF = 1$ results in a decelerated level-off segment; for an $ESF = 0$, the energy

rate budget is dedicated to the descent while the true airspeed remains constant. Then, any $ESF < 0$ provides a steep segment where part of the potential energy is transformed into kinetic energy. The lower bound on ESF has been set to -0.5 so that the value satisfies Eq.(18) and also prevents the aircraft from accelerating too much during descent. Moreover, airbrakes extension is limited between zero and the maximum deflection angle, which varies as a function of altitude and speed:

$$0 \leq \delta_{ab} \leq \delta_{ab_{\text{Full}}} \tag{21}$$

Finally, flap settings are changed according to the aerodynamic change configuration speed ($V_{CC_{ap}}$) for each flap deflection, as defined in the PDB:

$$\text{Conf} \in \{\text{clean}, 1, 2, 3, \text{Full}\} \tag{22}$$

## III. Trajectory Optimization Algorithm

The algorithm implemented for the computation of optimal trajectories is a version of A* [18] completely adapted and generalized [34] to comply with any existing arrival procedure, which assures that the path reaches the aircraft position. The stabilization point is the initial state of the algorithm and is generally defined as the point of a trajectory located 1000 feet above the runway [35], where the aircraft is in landing configuration as indicated in Fig. 1. Therefore, the calculation is performed upstream from that stabilization gate up to the current aircraft position, which defines a permanent optimal trajectory linking two particular energy states. In reality, the algorithm computes the optimal trajectory for any given initial and final state. The search space is incrementally generated from the initial node until the neighborhood area around the target state is reached. The generation of nodes is done through the discretization of control variables and accounts for the distribution of constraints for the construction and pruning of the search space. The A*-based algorithm prioritizes all nodes according to a certain score $f(n)$, which is the sum of the cost-to-go to from the initial to the current node $n$, represented by $g(n)$, and an estimation of the optimal cost from node $n$ to the target node, also known as the heuristic function $h(n)$.

$$f(n) = g(n) + h(n) \tag{23}$$

The heuristic function used by the A* algorithm is constructed on the basis of a constraint-less glide trajectory maintaining $V_{CAS_{Gdot}}$, defined as the speed which provides the best lift-to-drag ratio for a certain altitude and mass. The optimal cost estimation for each node of the search space is obtained by interpolation. The state variables of each node are the interpolation points whereas the output value is the fuel estimation. Both admissibility and consistency properties are satisfied as the function is optimistic (estimated cost is always lower than the actual optimal) and monotonically decreasing along the path. From the current node, next nodes are branched according to a certain

combination of controls. The pruning process is activated as soon as the next node intersects any constraint. At the end of the process, a node is added to the priority list if it satisfies all constraints, otherwise it is discarded. The node generation process is performed in an iterative way, the current node is the node in the priority list whose cost $f$ is minimum. It is continuously updated and its selection is independent of the position of the node with respect to the target, which means that the algorithm may branch a node at the beginning of the search space if it is the most promising one.. The principle of the pruning process in the presence of altitude and speed constraints is illustrated in Fig. 2, where the next generated node $n_{i+1}$ is the one colored in gray. The red cross symbol denotes the portion of the trajectory removed, since the intersection between the trajectory and the altitude constraint defines the actual next node $n_{i+1}$. Hence, the number of combinations and candidate states is reduced and nodes are generated at relevant locations of the search space.

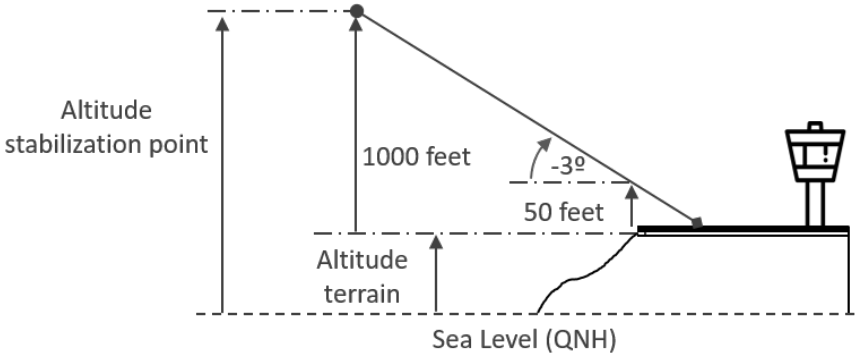


**Fig. 1 Definition of the stabilization point.**

The resulting search space at the end of the computation is displayed in Figs. 3 and 4, the algorithm terminates as soon as a node falls within the neighborhood zone around the target point and there is no more promising node in the priority list. From that node, parents are retrieved until the start node is reached. Children nodes are those that have been generated at those point of the calculation. Parent nodes are those generated nodes from where new children nodes have been developed. This implies that parent nodes have been at some point the most promising node in the priority list. The optimal altitude profile is the blue-dotted line shown in Fig. 3 whereas the optimal speed profile is the green-dotted line displayed in Fig. 4. In both figures, the initial and the final states are represented by magenta diamonds. The constraints (magenta triangles) prune the search space so that the resulting trajectory complies with the procedure design. The impact of constraints in the search space is observed in the range of -65NM to -120 NM, since no constraints apply and the number of combinations increase largely. From an operational point of view, flight crew would follow the computed path manually or automatically except when any circumstance forces the aircraft to deviate from the intended route. In that case, the calculation shall be relaunched to adapt the flight strategy to the dynamic aircraft state (tactical approach). In case that a solution does not exist due to the complexity of the procedure design

and aircraft performance, the algorithm explores all candidate nodes and produces an error message, resulting in too large computation times. Under these circumstances, flight crews may relax or disregard any constraint to ensure that the algorithm finds a solution. The computed trajectory corresponds to the global optimum as long as the heuristic is admissible and consistent.

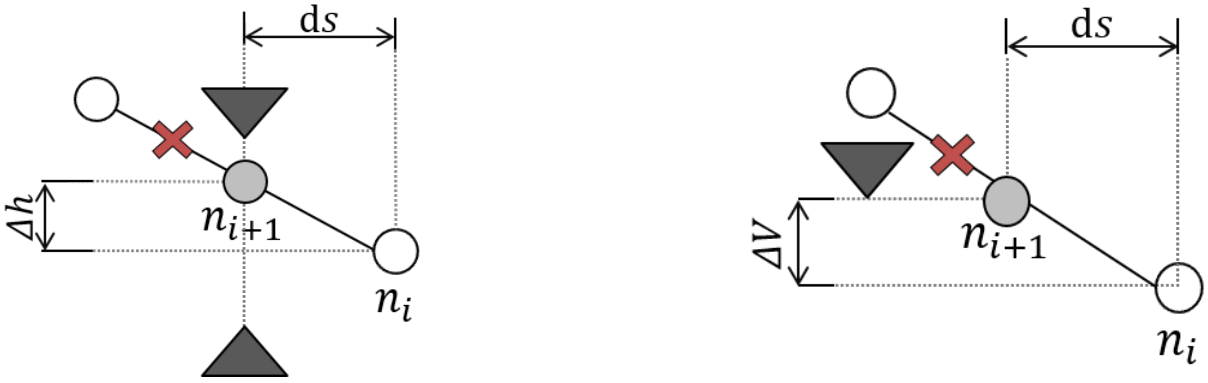


(a) Altitude constraint pruning.

(b) Speed constraint pruning.

**Fig. 2 Node generation process in the presence of constraints (gray triangles): a) Window altitude constraint, b) Speed constraint.**

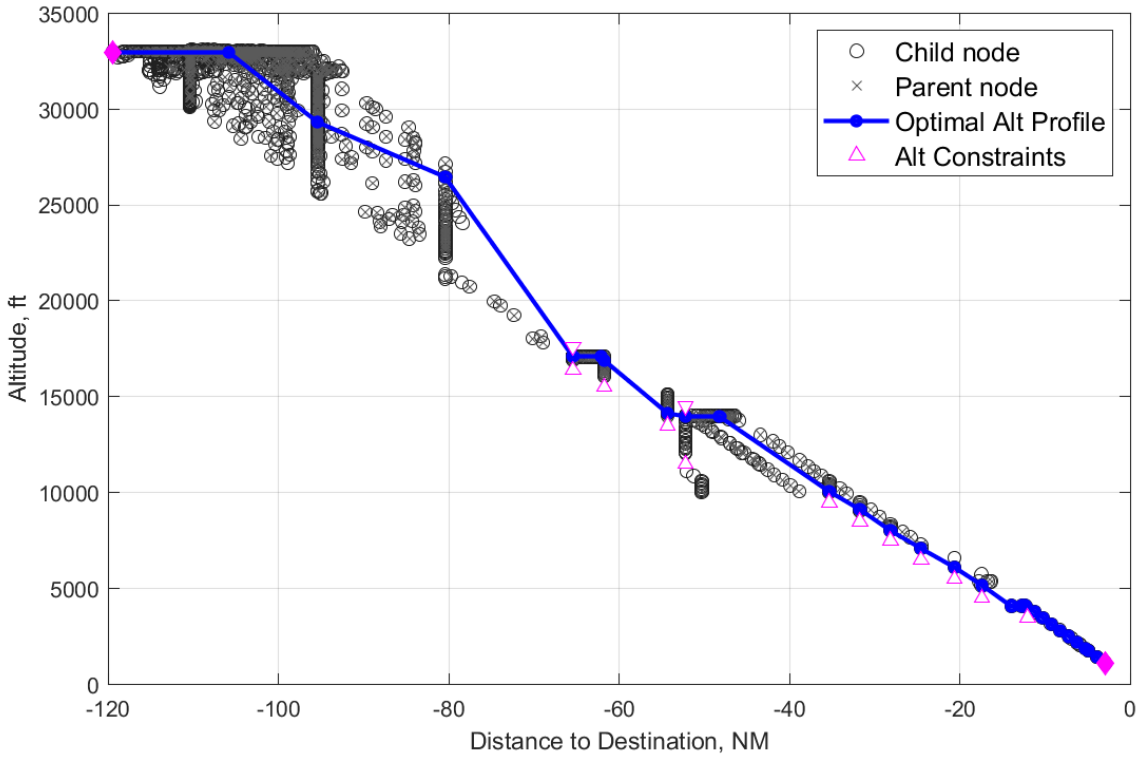


**Fig. 3 Search Space after calculation. The optimal altitude profile (blue-dotted line), children and parent nodes, altitude constraints (magenta triangles) and the initial and target nodes (magenta diamonds).**

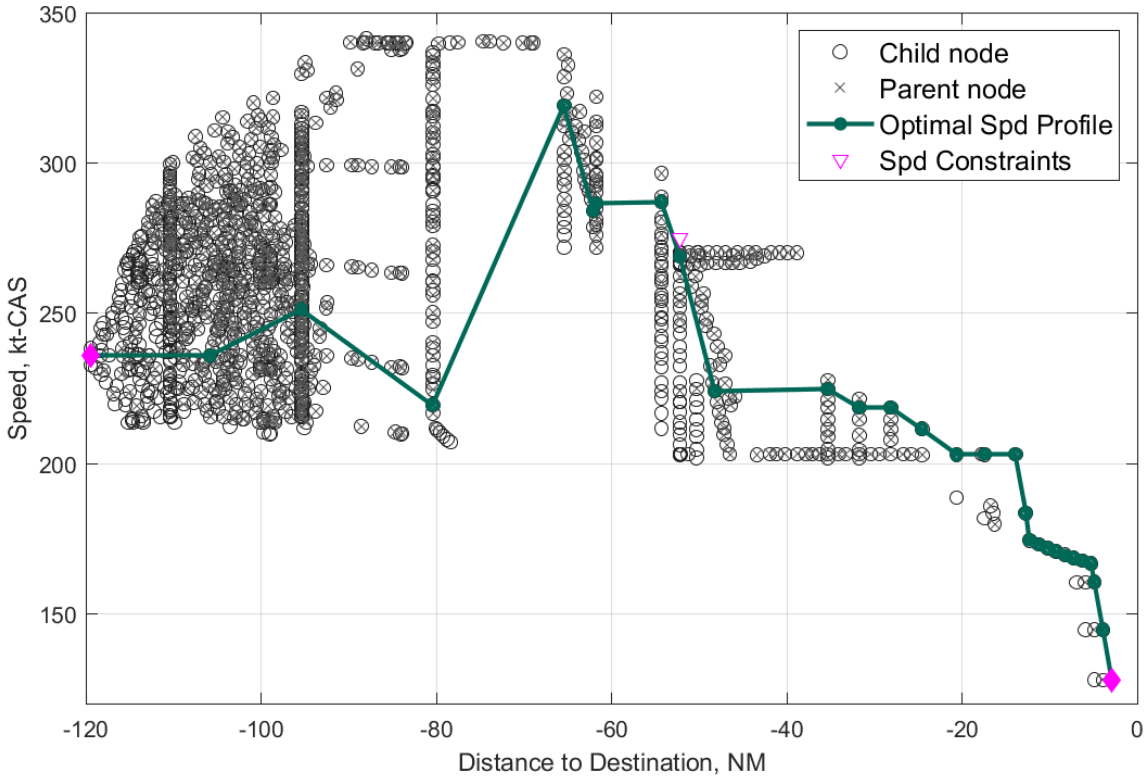


**Fig. 4 Search Space after calculation. The optimal speed profile (green-dotted line), children and parent nodes, speed constraints (magenta triangles) and the initial and target nodes (magenta diamonds).**

## IV. Results and Findings

### A. Trajectory Optimization at Los Angeles (KLAX) airport

This section presents and discusses the fuel-efficient trajectory obtained for an arrival procedure at Los Angeles (KLAX) airport. The trajectory is computed assuming that the aircraft is still on cruise phase. Then, it is compared with the one produced by a real FMS and tested in the Airbus flight simulator with the aim of assessing the operational concept. The selected aircraft model is the A320, since fuel savings in descent and approach phases represent a higher percentage of the total fuel spent for short-haul aircraft than for long-haul, and the figures are multiplied as soon as the number of operations per day and complete airline fleet are taken into account. The following Table 1 defines a set of parameters used for the calculation.

Where ΔISA is the temperature deviation relative to the international standard atmosphere. The aircraft is relatively heavy as the landing weight of 132 227 lb, which corresponds to 90% of the maximum landing weight (MLW), is a representative value of airlines operations. The selected Standard Terminal Arrival Route (STAR) procedure corresponds to that of an RNAV procedure at KLAX airport, called SEAVU2, as displayed in Fig. 5.

**Table 1 General parameters used for the calculation.**

| Parameters | |
|---|---|
| Aircraft type | A320 |
| Cost Index, lb/s | 0 |
| Gross weight, lb | 132 227 |
| Wind, ft/s | 0 |
| ΔISA, °K | 0 |

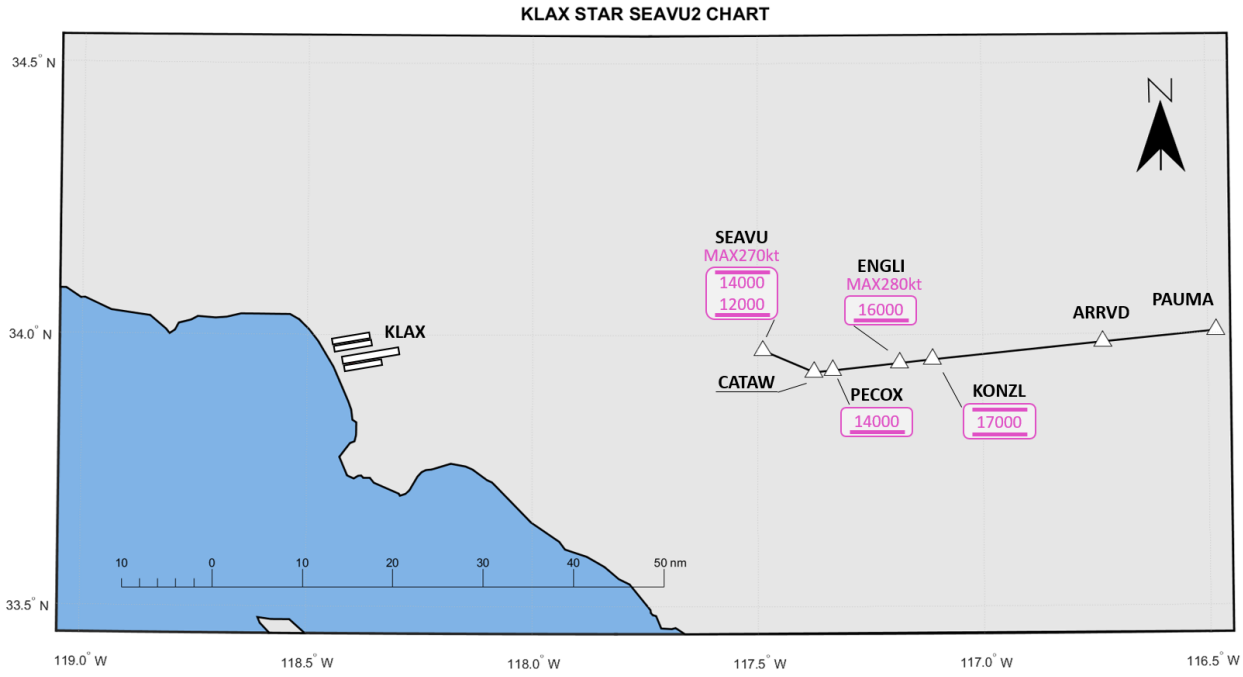


**Fig. 5 STAR SEAVU2.**

The altitude and speed constraints for each waypoint defined in the SEAVU2 STAR chart are summarized in table 2:

**Table 2 STAR SEAVU2 procedure constraints.**

| Waypoint | Type of constraint | Altitude, ft | Speed, KCAS |
|---|---|---|---|
| KONZL | AT | 17000 | n/a |
| ENGLI | AT OR ABOVE | >16000 | 280 |
| PECOX | AT OR ABOVE | >14000 | n/a |
| SEAVU | WINDOW | 14000-12000 | 270 |

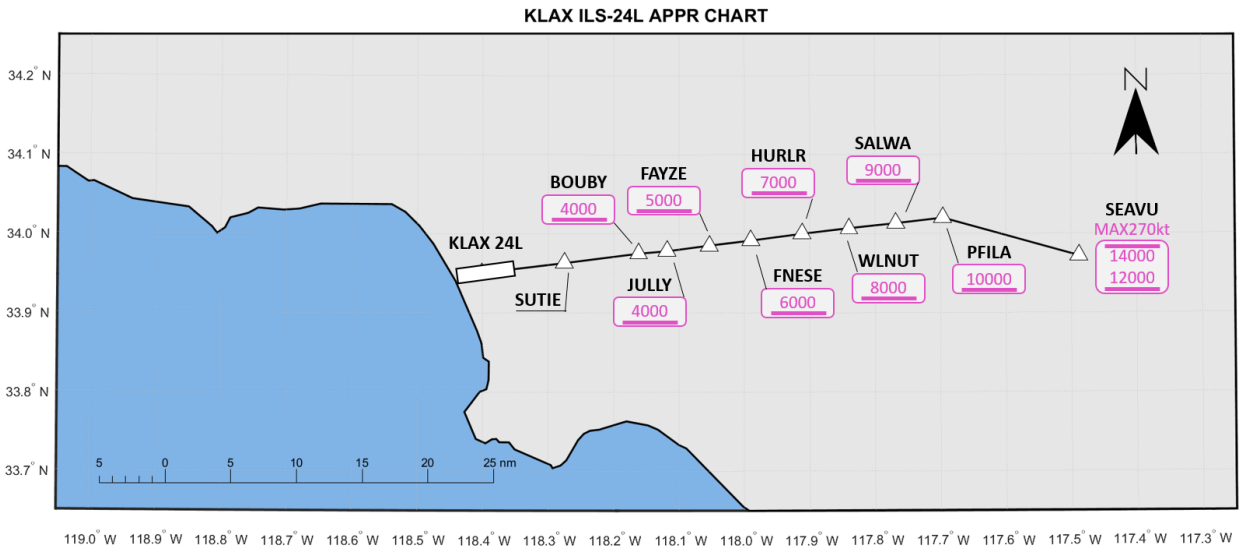


**Fig. 6 APPR ILS-24L.**

This procedure has been selected due to the number of constraints and the fact that track variations are small from the entry point to the runway. A standard precision approach (ILS-24L) to runway 24L has been selected, which is displayed in Fig. 6. Table 3 contains the constraints described in the approach chart:

**Table 3 ILS-24L procedure constraints.**

| Waypoint | Type of constraint | Altitude, ft |
|---|---|---|
| PFILA | AT OR ABOVE | >10000 |
| SALWA | AT OR ABOVE | >9000 |
| WLNUT | AT OR ABOVE | >8000 |
| HURLR | AT OR ABOVE | >7000 |
| FNESE | AT OR ABOVE | >6000 |
| FAYZE | AT OR ABOVE | >5000 |
| JULLY | AT OR ABOVE | >4000 |
| BOUBY | AT OR ABOVE | >4000 |

The initial and final conditions of the scenario are summarized in Table 4:

**Table 4 KLAX case study initial and final conditions.**

| State variable | Initial | Final |
|---|---|---|
| Distance to destination, NM | -116.5 | -2.95 |
| Altitude, ft | 33000 | 1125 |
| Speed, KCAS | 235 | 133.8 |
| Flap setting | Clean | Full |

### B. Trajectory comparison with a certified FMS

In this scenario, the A* algorithm computes the trajectory linking the top-of-descent location computed by a real-world FMS to the stabilization gate, which is usually located between the final approach fix and the runway threshold. The aircraft is assumed to be at the top-of-descent, since it enables the comparison between FMS performances and the calculation provided by the A* algorithm. Nevertheless, A* can compute the optimal trajectory for any given aircraft state while the FMS always calculates a top-of-descent, regardless of the actual aircraft position. The altitude and speed profiles computed by the algorithm are compared to those produced by a certified FMS, as it is displayed in Fig. 7. Similary, the optimal values of the control variables obtained from the A* calculation are compared with the values used by the FMS in Fig. 8.

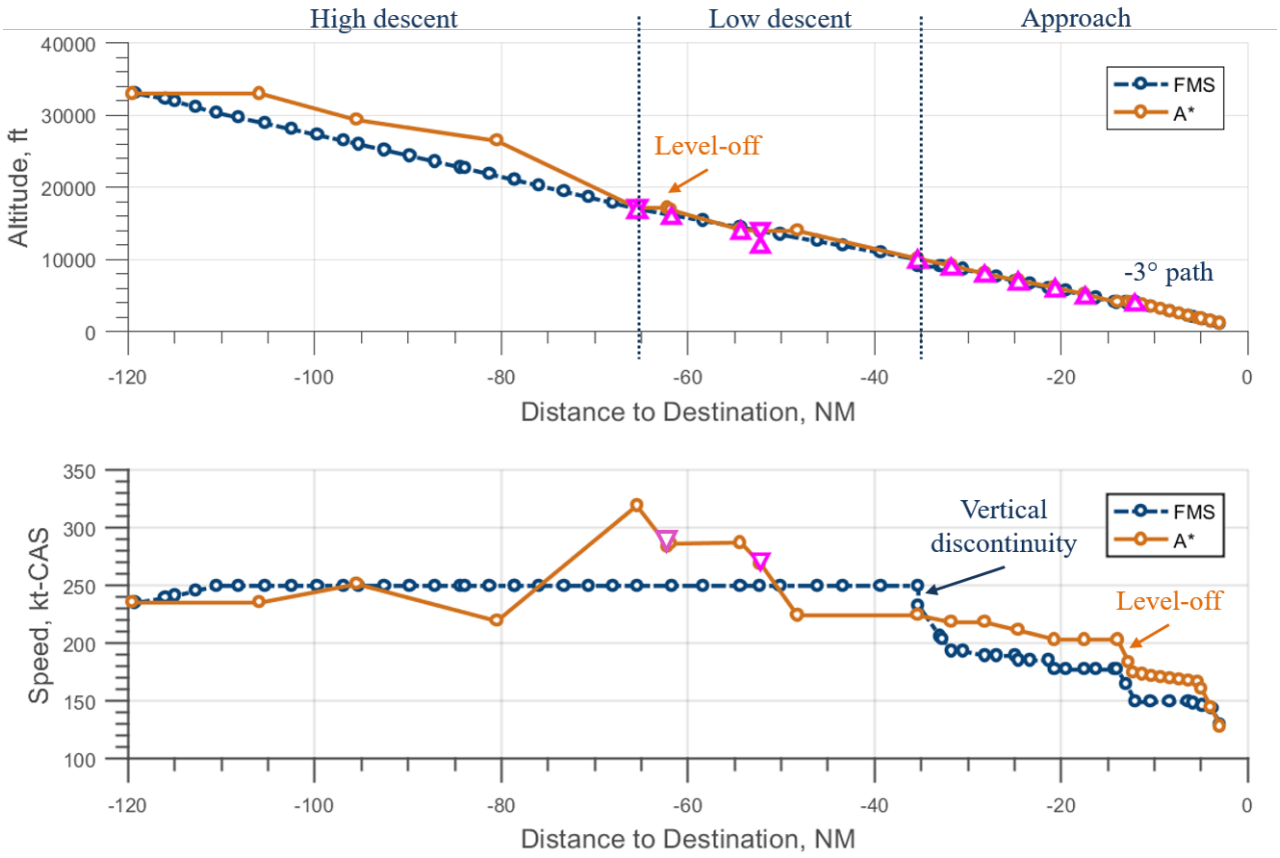


**Fig. 7 Comparison between the altitude and the speed profile computed by the A* algorithm and a certified FMS. Altitude constraints are displayed by pink triangles.**

Although the computation is performed backwards, the analysis of the trajectory will be done in the forward sense for clarity purposes. The trajectory is splited into three zones: the high descent, between the cruise level and the first altitude constraint, the low descent, between the first constraint and the initial approach fix, and the approach. In the high descent, the FMS maintains the Mach constant (CAS increases) until the crossover altitude is reached at 30000 ft.

Then, the CAS of 250 kt is maintained until the first altitude constraint at 17000 ft. In turn, the A*-computed trajectory stretches the cruise phase, and then the aircraft glides maintaining its speed in the range of 220-250 kt. From -80 NM until the first altitude constraint, the aircraft performs a steep descent where the speed increases up to 320 kt. At this waypoint, the total energy of the aircraft is higher in the A* trajectory than in the FMS one.

In the low descent, the different altitude constraints impose the construction of two consecutive constant flight-paths (i.e. geometric segment), the first from -65 NM to -61 NM and the second from -61 NM to -35 NM (see the value of $\gamma$ in Fig. 8, which is constant for the FMS trajectory). During the geometric segment thrust is higher than idle in order to keep the flight-path constant. Instead, the A* trajectory performs a decelerated level flight, descends at a constant speed of 275 kt and decelerates again from 275 kt to 220 kt at 12000 ft (upper bound on SEAVU altitude constraint). The level flights can be observed in Fig. 8, where the value of ESF is equal to one. When the speed reaches 220 kt, the aircraft glides at constant speed until reaching PFILA at -35 NM, which corresponds to the initial waypoint of the approach procedure.

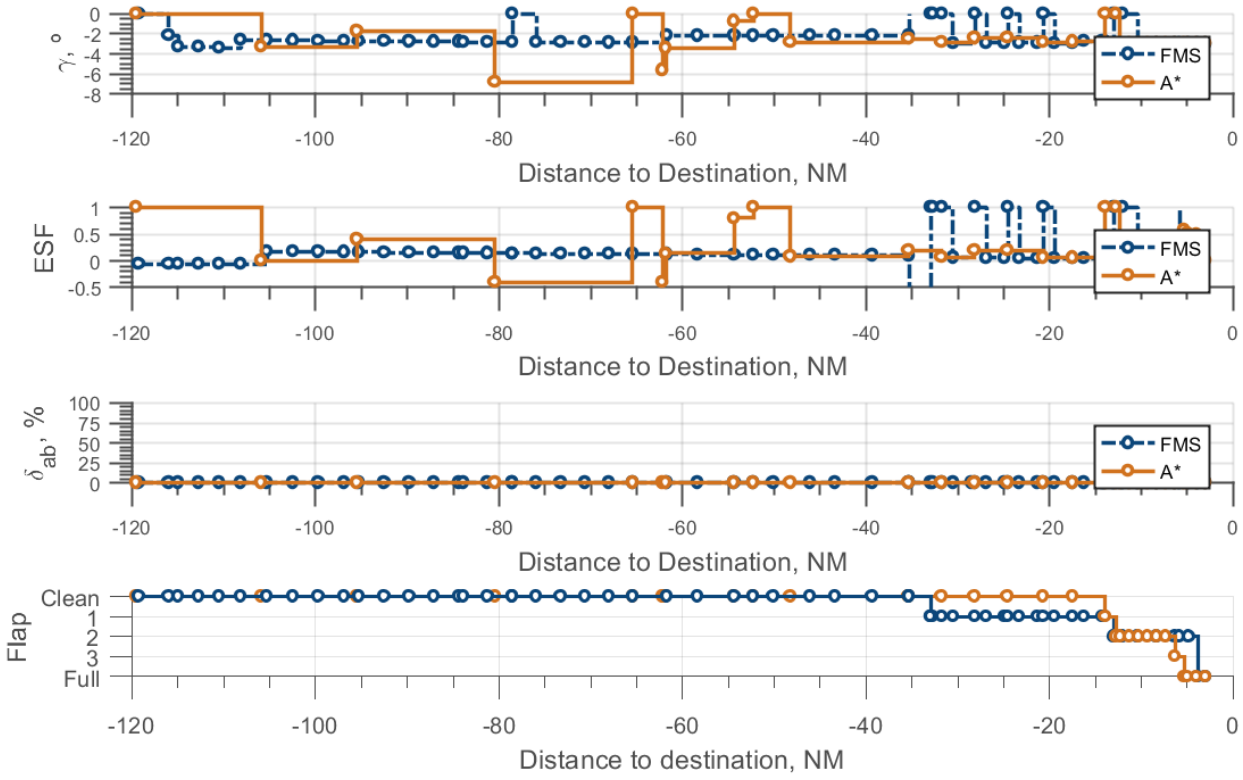


**Fig. 8 Comparison between flight controls computed by the A* algorithm and a certified FMS.**

Below 10000 ft, speed of 250 kt shall not be exceeded. A vertical discontinuity is clearly seen at -35 NM in the FMS speed profile shown in Fig. 7; the aircraft can not deccelerate and descend simultaneously to satisfy the constraints. The consecutive altitude constraints impose a certain flight-path where the aircraft decelerates slowly. As a consequence, flap setting 1 is extended earlier than in the A* trajectory (see $\delta_{ab}$ in Fig. 8), which results in a longer flown distance

with flaps set. Regarding the A* trajectory, the aircraft initiates the approach at lower speed and decelerates slightly at the same times as altitude constraints are satisfied. Then, the deceleration rate is increased as soon as flaps are extended during the level flight, which terminates when the FAF waypoint is reached. From that waypoint the aircraft keeps decelerating on a -3° FPA until reaching the stabilization gate. In the FMS, the speed at which flaps are extended is defined by the PDB, whereas in the A* trajectory the speed is defined by the algorithm. As a consequence, the FMS profile extends full flaps later, which results in a lower deceleration rate during the final approach in contrast to the A* profile. The increased deceleration rate during final approach and the fact that the algorithm does not follow constant flight-paths (geometric segments) imposed by the procedure avoid the construction of a vertical discontinuity.

For this case study, fuel consumption is reduced by 8% with respect to the FMS calculation whereas arrival time is as well decreased by 5%. In general, fuel savings are well localized; in this case, the shorter approach path and the removal of the geometric path, which occurs between -35 and -61 NM during the low descent are the causes of this decrease. Instead, the A* design divides constant FPA geometric segments into several segments, which yields a more efficient energy repartition that helps to maintain thrust idle as long as possible. In the A* profile, thrust is added during the high descent, stretching the cruise path. In turn, the FMS adds thrust during the low descent in order to maintain the shallow flight-path imposed by the altitude constraints. From a fuel consumption perspective, it is more efficient to add power during the high descent than during the low descent.

### C. Assessment of the trajectory in A320 simulator

The A*-computed trajectory was flown in a simulator at Airbus facilities to check that the behavior of the aircraft was consistent with the calculations. The integration points used by the algorithm were entered manually into the flight plan through their latitude and longitude coordinates, which helped to change the flight-path targets at the correct distance for the trajectory monitoring. Figure 9 shows the STAR procedures waypoints (green-diamond) and those computed by the A* (black-squared) that were stored in the FMS memory and entered in the flight-plan. As of today, there is no guidance mode that follows automatically the computed trajectory. Thus, the trajectory was tracked manually with autothrust off, thrust levers manually adjusted at idle setting and the auto-pilot switched on, in order to follow the lateral path defined by the arrival procedure. The vertical motion was managed by means of FPA adjustments performed at the locations defined by the algorithm. The lateral path is automatically managed by the auto-pilot (TRK target dashed) whereas the FPA target defines the rate of descent of the aircraft. Thrust was set to idle for the whole arrival procedure. With the vertical speed imposed by the FPA and thrust levers set to idle, the aircraft decelerated and accelerated accordingly.

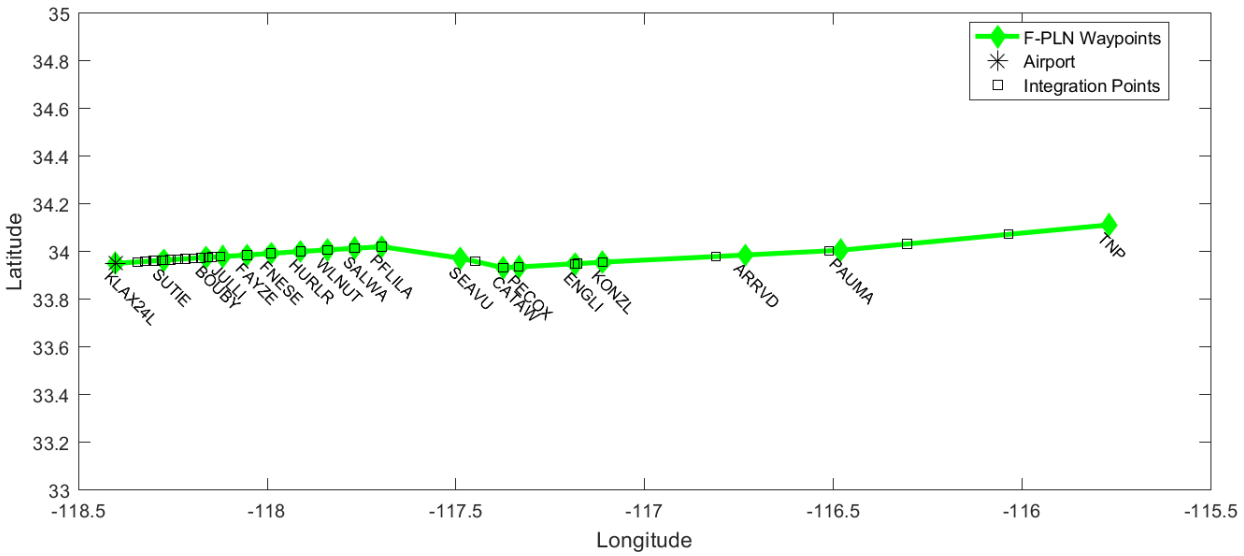


**Fig. 9 Flight plan preparation for KLAX arrival procedure. Integration points were inserted manually in the flight plan.**

The path-tracking was performed properly through successive FPA changes at the proper distance to the destination. The pilot-flying (PF) adjusted the FPA values on the FCU whereas the pilot non-flying (PNF) checked that the changes were done at the proper distance and that both the altitude and the speed profile was followed. It shall be noted that neither the PF nor the PNF are professional or flight test pilots but FMS engineers with sufficient knowledge and experience on auto-flight systems. As a general principle, transitions from shallow to steep paths were anticipated to limit over-shooting.

The comparison between the trajectory calculated by the algorithm and the one flown in the simulator is given as a function of time in Figs. 10 and 11. In general, the altitude profile was followed correctly. As it is observed in Fig. 10, the level-off computed at 17000 feet was initiated 1500 feet below, which resulted in an increase of speed above the calculated value (see Fig. 11). Then, several path adjustments corrected the situation without the need of airbrakes, the aircraft returned to the reference altitude and the speed profile. Nevertheless, from that point, deviations on the speed profile are observed, which results in a speed error of 5 knots at the end of the comparison (see Fig. 11). The post-session data analysis showed a difference of 1% between the fuel consumption computed by the A* algorithm and that consumed during the simulation test. This difference is likely to come from the deviation of the altitude profile due to the delayed level-off. This result confirms that fuel savings can be obtained by tracking the profile computed by the algorithm. From an operational perspective, this flight simulator evaluation suggests that further operational refinements should be considered in order to reduce the increased workload resulting from the continuous changes of FPA target, although the trajectories are physically flyable from a flight performance perspective.

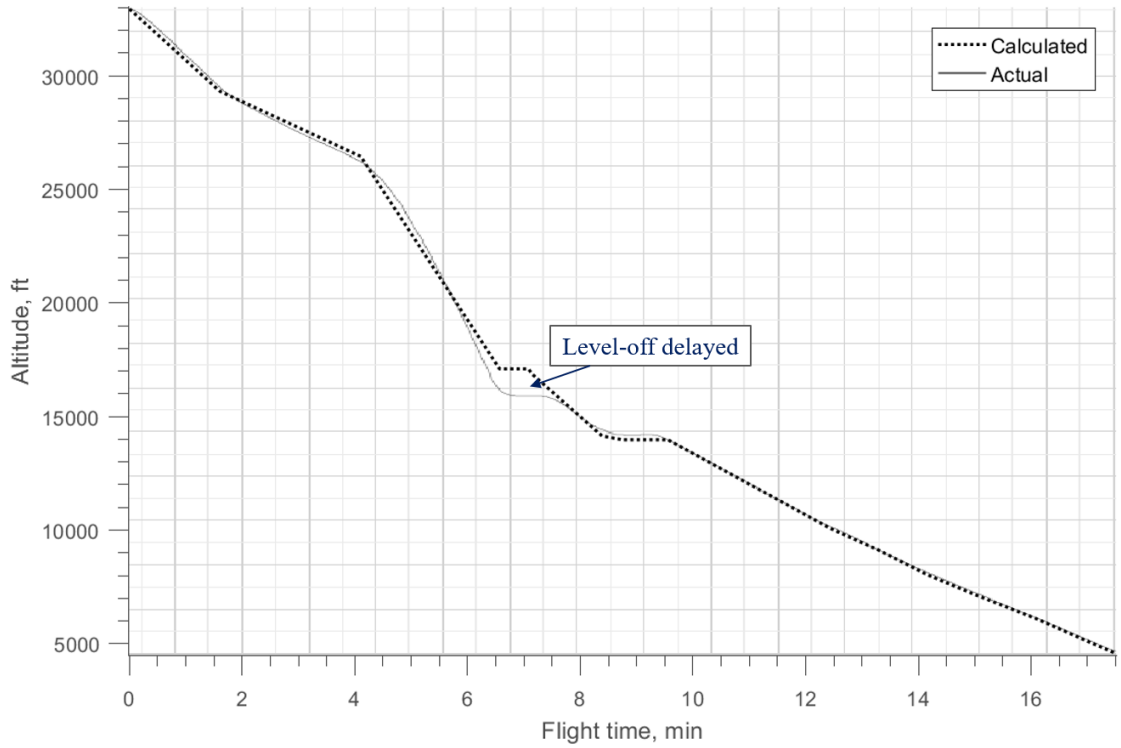


**Fig. 10 Comparison of the optimized altitude profile (dotted line) with the one flown in simulator (solid line).**

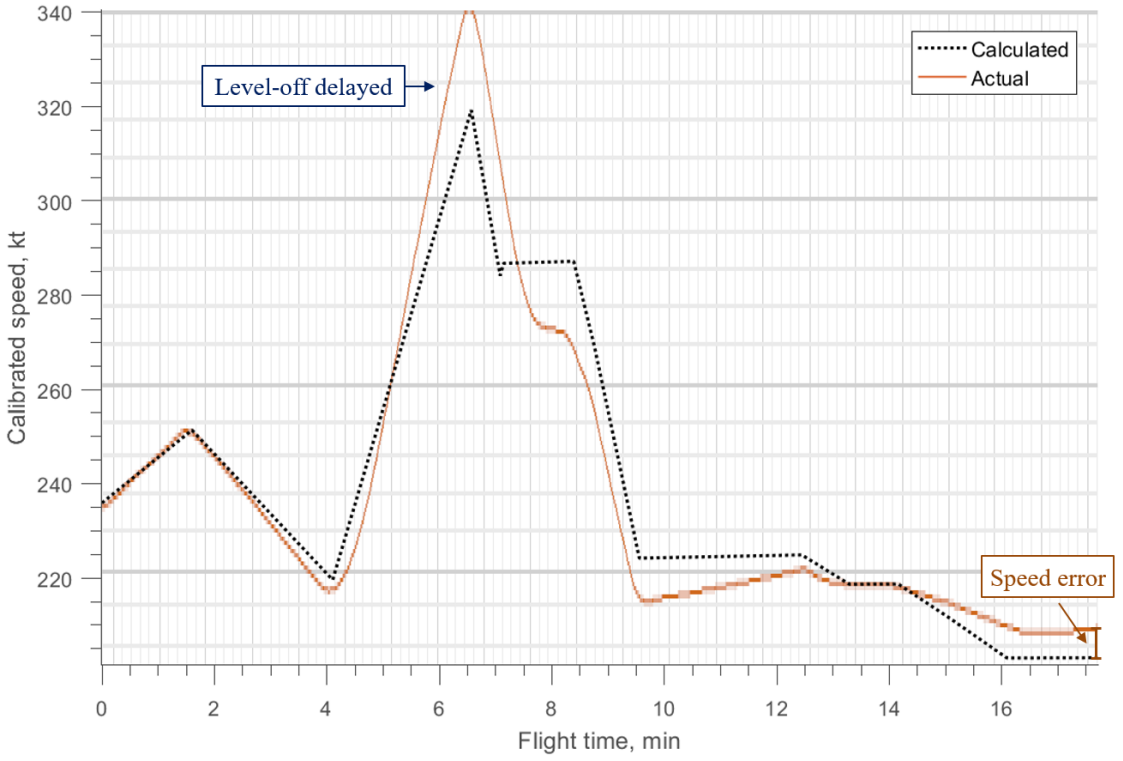


**Fig. 11 Comparison of the optimized speed profile (dotted line) with the one flown in simulator (solid line).**

The design and implementation of a guidance mode defined on the basis of the energy-sharing concept could automate this type of flight operations. From an air traffic perspective, the acceptance of variable optimal speed descent profiles instead of traditional Mach/CAS may depend upon the implementation of the trajectory information sharing from an aircraft to ground. These results constitute a solid background for the construction of fuel-efficient descent and approach profiles.

## V. Conclusion

This Note proposes an algorithm that computes, upstream, the fuel optimal trajectory for any published arrival procedure. The trajectory is permanent in the sense that it accounts for the current aircraft state regardless of the energy condition and guidance mode. Results show that 8% fuel savings can be obtained by the optimal trajectory solution in comparison to that computed by a state-of-the-art Flight Management System (FMS). As a side effect, flight time is reduced by 5%. The trajectory computed by the algorithm was tracked in an Airbus A320 flight simulator, equipped with certified avionic systems, with the aim of validating the operational feasability of the calculation. Post-simulation data analysis confirms the fuel savings computed by the algorithm. In addition, it suggests that the aircraft is capable of following the calculated profile with current guidance modes, although workload increases as a result of consecutive flight-path angle (FPA) changes. Furthermore, the A*-computed optimal trajectory produced no vertical discontinuities, unlike that computed by the state-of-the-art FMS. The computed optimal arrival profile suggests to accelerate or decelerate along the trajectory, which results in a variable calibrated airspeed (CAS) profile instead of a traditional Mach/CAS scheme defined by the FMS. The profile also complies with any arrival procedure or airline standard operating procedures constraints. In conclusion, the algorithm proposed in this Note yields the most fuel-efficient trajectory that reaches the current aircraft state, no matter what the energy condition or guidance mode is, and can be manually tracked with state-of-the-art guidance laws. Although the logics used in the algorithm are somehow complex to be onboarded in the current generation of FMS, some of the improvements disclosed in this Note could already be integrated in next FMS standards (e.g. logics for vertical discontinuity avoidance). Further research will focus on the integration of the algorithm with the FMS, and it will probably require a novel architecture in which the FMS interfaces with an external device with high processing power hosting the algorithm. Also, further investigation and evaluation with flight tests pilots will increase the maturity of the operational concept and will help to define novel flight controls and guidance laws that will enable the automatic tracking of the trajectory. The construction of optimal trajectories that take into account the current aircraft position on a real-time basis is an enabler for the development of more automated cockpits in the light of improving the efficiency of the flight.

## References


[1] Airbus (ed.), *Global Market Forecast 2019-2038 - Mapping Demand*, Airbus S.A.S. ISBN: 978-2-9554382-4-6, 1 Rond Point Maurice Bellonte, 31707 Blagnac Cedex, France, 2019.

[2] Eurocontrol (ed.), *European Aviation in 2040. Challenges of Growth*, Eurocontrol, Rue de la Fusee 96, 1130 Brussels, Belgium, 2018.

[3] EASA (ed.), *Continued Growth of Aviation poses Environmental Challenges*, European Aviation Environmental Report 2019, European Aviation Safety Agency, Konrad Adenauer Ufer 3, 50668 Cologne, Germany, 2019.

[4] Eurocontrol (ed.), *Free Route Airspace developments*, European Organisation for the Safety of Air Navigation, Rue de la Fusee 96, 1130 Brussels, Belgium, 2016.

[5] ICAO (ed.), *Continuous Descent Operations (CDO)*, Manual - Doc 9931 AN/476, International Civil Aviation Organization, 999 Robert-Bourassa Boulevard, Montreal, Quebec, Canada H3C 5H7, 2010.

[6] Fricke, H., Seis, C., and Herrmann, R., "Fuel and Energy Benchmark Analysis of Continuous Descent Operations," *Air Traffic Control Quarterly*, Vol. 23 No.1, 2015. https://doi.org/10.2514/atcq.23.1.83.

[7] Liden, S., "The evolution of Flight Management Systems," *AIAA/IEEE Digital Avionics System Conference 13th DASC*, Vol. 21, No. 11, Oct. 1994. https://doi.org/10.1109/DASC.1994.369487.

[8] Spitzer, C. R. (ed.), *The Avionics Handbook*, 3rd ed., The Electrical Engineering Handbook Series, chapter and pages, pp. 15, 153–178.

[9] Airbus (ed.), *Descent and Approach Profile Management*, Flight Operations Briefing Notes, Airbus S.A.S, 1 Rond Point Maurice Bellonte, 31707, Blagnac Cedex France, Oct. 2006.

[10] Airbus (ed.), *Aircraft Energy Management during Approach*, Flight Operations Briefing Notes, Airbus S.A.S, 1 Rond Point Maurice Bellonte, 31707, Blagnac Cedex France, Oct. 2005.

[11] Betts, J. T., and Cramer, E. J., "Application of direct transcription to commercial aircraft trajectory optimization," *Journal of Guidance, Control and Dynamics*, Vol. 18, No. 1, 1995, pp. 151–159. https://doi.org/10.2514/3.56670.

[12] Delahaye, D., Puechmorel, S., Tsiotras, P., and Feron, E., "Mathematical Models for Aircraft Trajectory Design : A Survey," *Electronic Navigation Research Institute (eds) Air Traffic Management and Systems. Lecture Notes in Electrical Engineering, vol 290*, 2014, pp. 205–247. https://doi.org/10.1007/978-4-431-54475-3_12.

[13] De Jong, P. M. A., De Gelder, N., Bussink, F. J. L., Verhoeven, R. P. M., Kohrs, R., and Mulder, M., "Time and Energy Management during Descent and Approach for Aircraft: Batch-Simulation Study," *Journal of Aircraft*, Vol. 52, No. 1, 2013. https://doi.org/10.2514/1.C032668.

[14] Park, S. G., and Clarke, J. P., "Vertical Trajectory Optimization for Continuous Descent Arrival Procedure," *AIAA Guidance, Navigation, and Control Conference*, 2012. https://doi.org/10.2514/6.2012-4757.

[15] Park, S. G., and Clarke, J. P., "Vertical Trajectory Optimization to Minimize Environmental Impact in the Presence of Wind," *Journal of Aircraft*, Vol. 53, No. 3, 2016. https://doi.org/10.2514/1.C032974.

[16] Fernandes, R., and Beskens, C., "Benefits of Optimal Flight Planning on Noise and Emissions Abatement at the Frankfurt Airport," *AIAA Guidance, Navigation and Control Conference*, 2012. https://doi.org/10.2514/6.2012-4482.

[17] Abdelmoula, F., and Scholz, M., "LNAS - A Pilot Assistance System for Low-Noise Approaches with Minimal Fuel Consumption," *31st Congress of the International Council of the Aeornautical Sciences*, Belo Horizonte, Brasil, 2018.

[18] Peter E. Hart, B. R., Nils J.Nilsson, "A formal Basis for the Heuristic Determination of Minimum Cost Paths," *IEEE Transactions of systems science and cybernetics*, Vol. SSC-4, NO.2, 1968. https://doi.org/10.1109/TSSC.1968.300136.

[19] Devulapalli, R., "An Efficient Algorithm for Commercial Aircraft Trajectory Optimization in the Air Traffic System," 2012. URL http://hdl.handle.net/11299/140007.

[20] E. Rippel, A. B.-G., and Shimkin, N., "Fast Graph-Search Algorithms for General Aviation Flight Trajectory Generation," *Journal of Guidance, Control and Dynamics*, 2005. https://doi.org/10.2514/1.7370.

[21] J. Doebbler, J. V., P. Gesting, "Real-time Path Planning and Terrain Obstacle Avoidance for General Aviation Aircraft," *AIAA Guidance, Navigation, and Control Conference and Exhibit. AIAA 2005-5825*, 2005. https://doi.org/10.2514/6.2005-5825.

[22] Zhao, Y., and Tsiotras, P., "Analysis of Energy-Optimal Aircraft Landing Operation Trajectories," *Journal of Guidance, Control and Dynamics*, Vol. 36, No. 3, 2013. https://doi.org/10.2514/1.57779.

[23] Zhao, Y., and Tsiotras, P., "Time-Optimal Path Following for Fixed-Wing Aircraft," *Journal of Guidance, Control and Dynamics*, Vol. 36, No. 1, 2013. https://doi.org/10.2514/1.57471.

[24] Zhao, Y., and Tsiotras, P., "Fuel-Efficient Flight Optimization for ATC Operations During Descent and Approach Phases," *AIAA Guidance, Navigation and Control (GNC) Conference*, 2013. https://doi.org/10.2514/6.2013-4539.

[25] Nelson R. Zagalski, R. P. I., and Schultz, R. L., "Energy state approximation and minimum-fuel fixed-range trajectories," *Journal of Aircraft*, Vol. 8 No. 6, 1971. https://doi.org/10.2514/3.44282.

[26] Calise, A. J., "Optimization of aircraft altitude and flight-path angle dynamics," *Journal of Guidance, Control and Dynamics*, Vol. 7 No. 1, 1984. https://doi.org/10.2514/3.8554.

[27] Erzberger, H. (ed.), *Automation of On-Board Flightpath Management*, NASA-TM- 84212, 1981.

[28] Erzberger, H., and Lee, H., "Constrained Optimum Trajectories with Specified Range," *Journal of Guidance, Control and Dynamics*, Vol. 3 No. 6, 1980. https://doi.org/10.2514/3.55950.

[29] Calise, A. J., "Extended Energy Management Methods for Flight Performance Optimization," *13th Aerospace Sciences Meeting*, 1975. https://doi.org/10.2514/6.1975-30.

[30] Andreu-Altava, R., Mere, J., Delahaye, D., and Miquel, T., "Graph-Search Descent and Approach Trajectory Optimization Based on Enhanced Aircraft Energy Management," *AIAA Aviation Forum 2019,*, 17-21 June 2019. https://doi.org/10.2514/6.2019-3618.

[31] L.Schultz, R., and R.Zagalsky, N., "Aircraft Performance Optimization," *Journal of Aircraft*, Vol. 9, No. 2, 1972. https://doi.org/10.2514/3.44326.

[32] ARINC (ed.), *Navigation System Database*, Aeronautical Radio Incorporated, ARINC Specification 424-22, 2018.

[33] Eurocontrol (ed.), *User Manual For the Base of Aircraft Data (BADA)*, Revision 3.9: EEC Technical/Scientific Report No. 11/03/03-03, Eurocontrol Experimental Center (EEC), 2011.

[34] Andreu-Altava, R., Mere, J., Delahaye, D., and Miquel, T., "Flight Management System Pathfinding Algorithm for Automatic Trajectory Generation," *37th Digital Avionics System Conference, London, UK*, 2018. https://doi.org/10.1109/DASC.2018.8569254.

[35] ALAR (ed.), *Stabilized Approach*, Flight Safety Foundation FSF ALAR Briefing Note 7.1, 2009.

## List of changes